

Synthesis, characterisation and ethanol sensing applications of MoO₃ – MoO₂ nanostructures at room temperature

D. Sudha^a, K. Uthayarani^{a,*}, N. Neelakandeswari^b, K. Jeyadheepan^c, M. Chitra^a

^a*Department of Physics, Sri Ramakrishna Engineering College, Vattamalaipalayam, Coimbatore 641022, India*

^b*Department of Chemistry, Nallamuthu Gounder Mahalingam College, Pollachi 642 001, India*

^c*School of Electrical and Electronics Engineering, SASTRA University, Tirumalaisamudram, Thanjavur 613 401, India*

In the present work, MoO₃ - MoO₂ nanocomposite is synthesised via hydrothermal method and is characterised using various state-of-the-art techniques. The high crystallinity of the sample is observed from XRD and FESEM reveals the 2D plate like layered structures with hexagonal facets. The prepared composite is subjected to ethanol sensing at room temperature and it is observed that the material exhibits 4.5% for 25 ppm ethanol with response time as 98 s and recovery time as 219 s. The observed small response of the composite material MoO₃ – MoO₂ with longer response-recovery time might be due to the large sized fibrils observed.

(Received August 14, 2023; Accepted November 23, 2023)

Keywords: Molybdenum oxide, hydrothermal, Ethanol, Sensitivity, Room temperature

1. Introduction

Transition metal oxides like chromium oxide, tungsten oxide, vanadium oxide, molybdenum oxide formed by 2D / 3D framework of octahedra or tetrahedra results in complex structures [1 - 4]. Among these common metal oxides, a low cost and low toxic ‘Molybdenum oxide’ exists in various compositions with multiple valence states from stoichiometric molybdenum oxide (MoO₃) to partially reduced MoO_{3-x} (2 < x < 3). Molybdenum trioxide (MoO₃) exists in three phases - a thermodynamically stable orthorhombic phase (α - MoO₃), a metastable monoclinic phase (β - MoO₃) and a hexagonal phase (h-MoO₃) [1, 4]. MoO₃, an n-type semiconductor with band gap 3.2 eV [5] is a pioneer component with rich structural polymorphism and stable bilayered structure held by van der waal forces [6]. The redox reactions and van der waals gap between octahedran Mo-O sheets in MoO₃ favours superior ion intercalation capability resulting in various applications like catalysis, display devices, petroleum refining, gas sensor devices, photoluminescence, etc [1, 7]. The band gap of the material could also be modulated due to the presence of oxygen vacancies. Because of the unique double layer structure, MoO₃ possess high theoretical capacity, high chemical and thermal stability. But MoO₃ in bulk form is limited due to low electrical conductivity, slow ion diffusivity which results in rapid capacity fading and lower capacity [4]. MoO₂ possess a strong metallic Mo-Mo bond resulting in good electrical conductivity even at room temperature. The morphological evolution [6 - 11] of molybdenum oxides (MoO₂ and MoO₃) with different nanostructures have been identified as the suitable promising candidates for device fabrication especially gas sensing applications.

* Corresponding author: uthayarani.karunakaran@srec.ac.in
<https://doi.org/10.15251/DJNB.2023.184.1451>

Nowadays, the demand for an efficient chemical sensor is the need of the hour to monitor the environment to protect the 'Mother Earth' from pollution and hazards. Some volatile organic compounds (VOCs) like acetone, alcohol and ammonia [12 - 15] which are present in our breath have to be checked for their higher dosage. Among these VOCs, ethanol detection [13, 16] from the drunken drivers as well as to control the fermentation process is required. Identifying the single target analyte amidst other volatiles is a challenge put forth to the researchers. In this present work, $\text{MoO}_3 - \text{MoO}_2$ nanocomposite is prepared using hydrothermal route, characterised using various state-of-the-art techniques and subjected to ethanol sensing applications at room temperature.

2. Experimental

The chemicals used for the synthesis of composite are ammonium molybdate ($(\text{NH}_4)_6\text{Mo}_7\text{O}_{24}$), nitric acid (HNO_3), citric acid monohydrate ($\text{C}_6\text{H}_8\text{O}_7 \cdot \text{H}_2\text{O}$) and ethanol ($\text{C}_2\text{H}_5\text{OH}$). All the chemicals are purchased from Sigma Aldrich and are used as such without further purification. The experimental procedure carried out is explained in Fig. 1. Initially, 0.1 M ammonium molybdate is prepared and required amount of nitric acid is added dropwise upon stirring until the pH reaches 1. After 1 hour of stirring, the mixture becomes transparent yellow solution. Next, 0.01 M solution of citric acid monohydrate is prepared and is added to the first solution. Then the solution is transferred to a teflon lined stainless steel autoclave and is heated in an oven at 150 °C for 24 h. After that the product is washed repeatedly with nitric acid, deionised water and ethanol several times. The resultant product is dried at room temperature and the product obtained is $\text{MoO}_3 - \text{MoO}_2$.

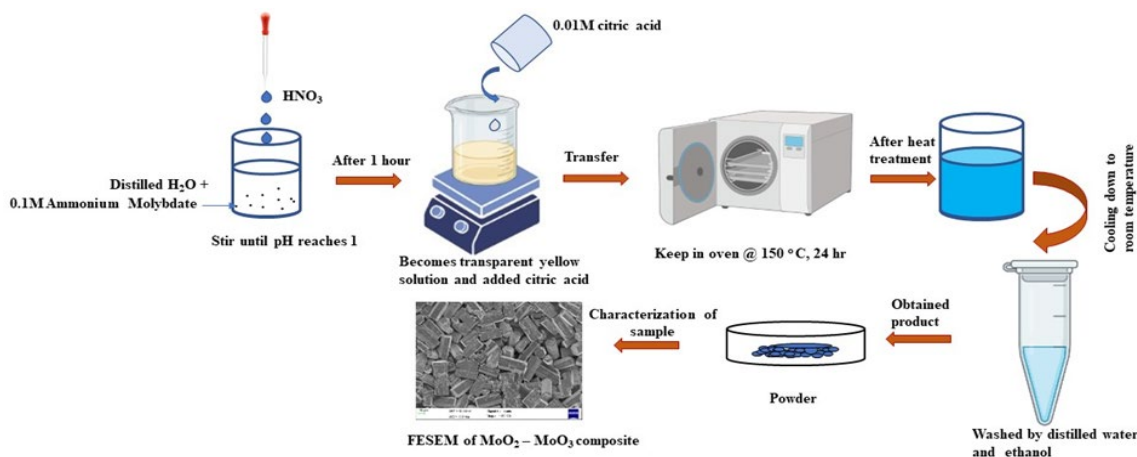


Fig. 1. Schematic representation for the synthesis of $\text{MoO}_3 - \text{MoO}_2$ composite.

The prepared sample is characterized systematically. The crystallite structure and phase composition is identified by X-ray powder diffraction (XRD) pattern obtained using PANalytical X'pert PRO X-ray diffractometer with Cu-K α radiation ($\lambda = 1.5406 \text{ \AA}$) as X-ray source. The vibrational modes present is obtained by ATR (Attenuated Total Reflectance) spectra recorded using Alpha T –Bruker. The morphology of the prepared sample is obtained from scanning electron microscopic (SEM) image using SIGMA WITH GEMINI COLUMN MODEL, CARL ZEISS (USA) make, Resolution 1.5 field emission Scanning Electron Microscope (FESEM). The purity of the prepared sample is obtained using Nano XFlash Detector MODEL, BRUKER (GERMAN) MAKE Energy Dispersive X-ray (EDAX) Spectrometer. The absorption spectra of the sample are obtained using Cary 60 UV-Visible spectrophotometer make Agilent technology and the band gap is calculated. The indigenous gas sensing set-up [17, 18] is used to carry out the sensing studies along with Keithley 2450 digital interactive source meter along with the computer running LabVIEW and control module.

3. Results and discussion

3.1. Structural properties

3.1.1. XRD

From the XRD pattern of the prepared sample (Fig. 2), the peaks are observed at 26.02 °, 31.21 °, 49.11 °, 50.08 °, 53.20 °, 67.24 °, 72.39 °, 79.39 ° and these peaks match with the ICDD 86-0135 corresponding to MoO₂ structured in Monoclinic.

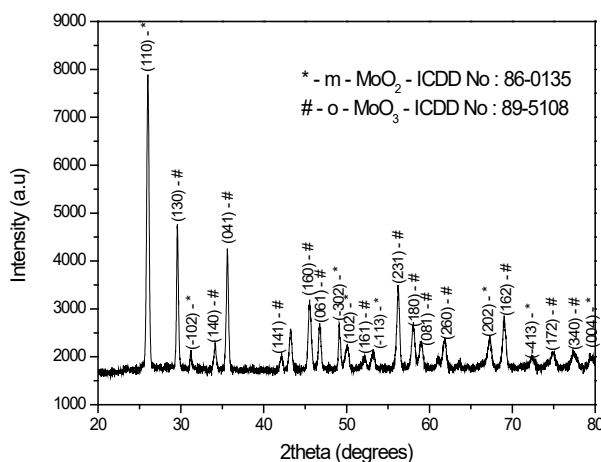


Fig. 2. XRD pattern of MoO₃ – MoO₂ composite.

The peaks observed at 29.58 °, 34.13 °, 35.62 °, 42.06 °, 43.23 °, 45.46 °, 46.69 °, 51.92 °, 56.19 °, 58.05 °, 58.91 °, 61.02 °, 61.85 °, 69.01 °, 74.77 °, 77.35 ° match well with ICDD No 89 - 5108 corresponding to orthorhombic MoO₃ [1]. The intensity of the peaks are high which reveals the crystalline nature of the sample. The crystallite size of the sample is calculated using Scherrer formula [16]

$$D = \frac{K \lambda}{\beta c \theta} n_s \quad (1)$$

where K is broadening constant (~0.9 assuming the particles are spherical), λ is the wavelength of CuK α radiation (1.54×10^{-10} m), β is Full width at Half maximum (FWHM) (in radian) and θ is the angle of diffraction (in °). The crystallite size obtained for the composite sample is calculated as 63.09 nm. The phase composition of the composite MoO₂ – MoO₃ was calculated using the formula [16]

$$\text{Phase composition} = \frac{I_{(hkl)}}{\sum I_{(hkl)}} \quad (2)$$

where $I_{(hkl)}$ is the intensity of the phase of interest and $\sum I_{(hkl)}$ is the sum of the intensities of all the phases. It is observed from XRD analysis that 34 % of MoO₂ and 66 % of MoO₃ are present in the composite.

3.1.2 FTIR

FTIR spectra recorded between 500 – 4000 cm⁻¹ of mixed phase of MoO₂ – MoO₃ are presented in Fig. 3. Three characteristic strong vibration modes at about 684, 901 and 972 cm⁻¹ were observed. The sharp absorptions at 972 and 901 cm⁻¹ are associated with stretching vibrations of the Mo=O bonds of layered α -MoO₃ phase [19 - 21] whereas the peak at 684 cm⁻¹ which is responsible to stretching mode vibration of Mo-O bonds of rutile structure of β -MoO₂ [22]. The wavenumbers

at 1405, 1699, 2308, 2631, 2880, 3214 and 3410 cm^{-1} are due to different stretching and bending vibrations of absorbed water respectively..

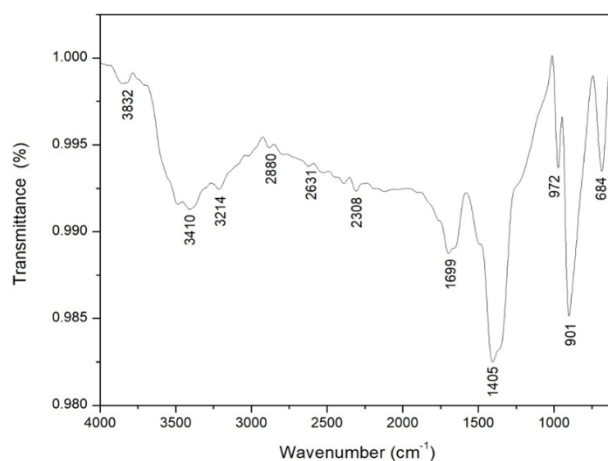


Fig.3. ATR-FTIR analysis of MoO_x ($\text{MoO}_2 - \text{MoO}_3$).

3.2. Morphological studies

3.2.1 FE-SEM

FE-SEM image of the prepared composite material under lower magnification as in Fig. 4 (a) shows the 2D plate like layered structures with length around 30 μm and width around 15 μm with hexagonal facets (shown as enlarged image). [23].

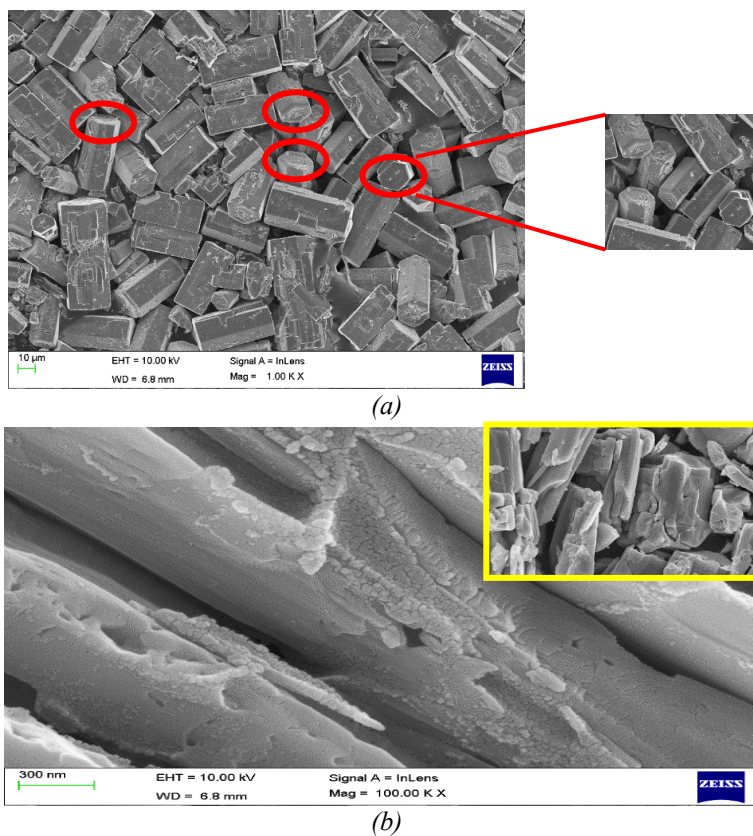


Fig. 4. FE-SEM image of $\text{MoO}_3 - \text{MoO}_2$ composite under (a) lower magnification (inset: hexagonal facets) and (b) higher magnification.

This is in accordance with the formation of stable orthorhombic phase as evidenced in the XRD pattern. Under higher magnification as in Fig. 4 (b), aggregates of nanofibrils resulted in microrods were observed [7]. These plates would have been held by the Van der Waals forces on the top of the layered structure resulting in the formation of lamellar patterns.

3.2.2. Optical properties

UV-Vis absorption spectra of $\text{MoO}_3 - \text{MoO}_2$ nanocomposite is depicted in the Fig. 5. Reports on optical band gap are available for individual MoO_3 nanobelts and MoO_2 microstructures as 3.04 eV and 4.22 eV respectively. In the present work, $\text{MoO}_3 - \text{MoO}_2$ nanocomposite absorbs UV light and shows low absorption in visible and near infrared regions [24 – 27]. One absorption edge occurs around 385 nm owing to the characteristic of MoO_3 which is a wide band gap semiconductor material. On the other hand a broad light absorption form UV to near infra red occurs due to the metallic property arises from MoO_2 . This could be attributed to the localized surface plasmon resonance in the nanocomposite. [24, 26 - 28].

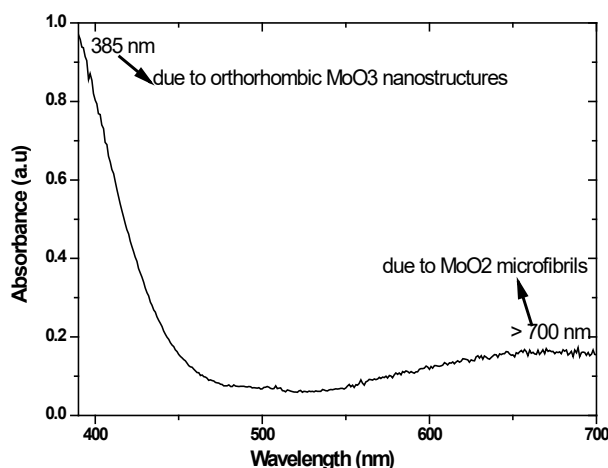


Fig. 5. UV – Vis absorption spectra of $\text{MoO}_3 - \text{MoO}_2$ composite under (a) lower magnification (inset: hexagonal facets) and (b) higher magnification.

3.3. Gas sensing analysis

The chemicals purchased from Merck were used for gas sensing analysis and were vaporised using flash vaporiser. A chamber with a capacity of 6 litres was taken; made air tight; and the valves were fitted with gas / vapour inlet and outlet controlled by solenoids. The material coated on the glass substrate of size 20 mm x 10 mm was kept on the sample holder and the ohmic contact was taken using the silver paste on the edges of the film surface [17]. The gas sensing experiments were carried out at room temperature and the resistance of the sensor element was measured by using Keithley 2450 interactive digital source measure unit for every 0.5 seconds by sourcing the voltage and measuring the current. The entire set up was controlled by a computer which runs under GUI developed in LabVIEW.

The concentration of the testing gas was calculated using the formula [18] –

$$C_{ppm} = \frac{\delta x V x R x T}{M x P_b x V_b} x 10^6 \quad (3)$$

where δ corresponds to the density of the testing gas (in g ml^{-1}), V is the volume of the injected gas (in μl), R is universal gas constant, T is the temperature of the sensor (in K), M is the molecular weight of the testing gas (in g mol^{-1}), P_b is the pressure of the chamber, V_b is the volume of the chamber (in litres).

3.3.1. Sensitivity

The gas sensitivity of the thin film sensor is determined by the change in resistance experienced by the sensor element when exposed to the particular gas. The chemisorption is observed on the surface of the thin film and the resistance changes and the normalized change in resistance is called the sensitivity of the sensor. The resistance of the sensor under ambient air condition was taken as the base line resistance and after stabilization, the vapour was injected through the inlet valve and the resistance change suffered by the sensor is determined using Keithley source meter. The sensitivity [16] was calculated using the formula –

$$\text{Response magnitude} = \frac{|R_{\text{air}} - R_{\text{ethanol}}|}{R_{\text{air}}} \times 100 \quad \dots\dots\dots(4)$$

which is described as the ratio of the modulus of magnitude of change in resistance upon exposure to ethanol vapour (R_{ethanol}) to that of in air without vapour (R_{air}). In the present study, all the gases acetone, ammonia, ethanol and methanol were tested at room temperature which aids in portability as well as reduces the cost in fabricating the microheater arrangement for increasing the temperature of the sensor. The sensitivity of the composite material towards ethanol for various ppm such as 5, 10, 25, 40, 50, 75, 100, 125, 150 and it is observed that the sensor response is around 4.5 % towards 25 ppm of ethanol at room temperature.

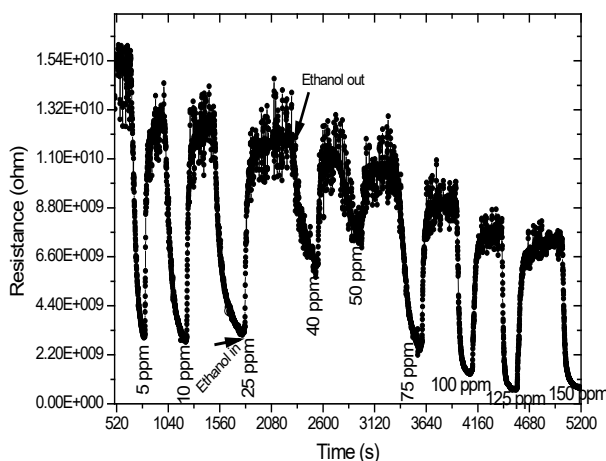


Fig. 6. Response – Recovery characteristics of $\text{MoO}_3 - \text{MoO}_2$ composite.

3.3.2. Response time and Recovery time

The response time is defined as the time needed to reach 90% of the base line resistance after the injection of the test gas and recovery time is defined as the time needed to reach 10% of the base line resistance after removal of the test gas and they were calculated from the time versus voltage plot [16]. The response time is calculated as 98 s and recovery time as 219 s for $\text{MoO}_3 - \text{MoO}_2$ sensor.

3.3.3. Selectivity

The selectivity is the ability of the sensor to detect the particular gas amidst other gases such as acetone, ammonia, ethanol and methanol. The sensitivity of the sample towards other gases is shown in Fig. 7 and it is observed that $\text{MoO}_3 - \text{MoO}_2$ exhibits comparatively pronounced sensitivity towards ethanol rather than other gases.

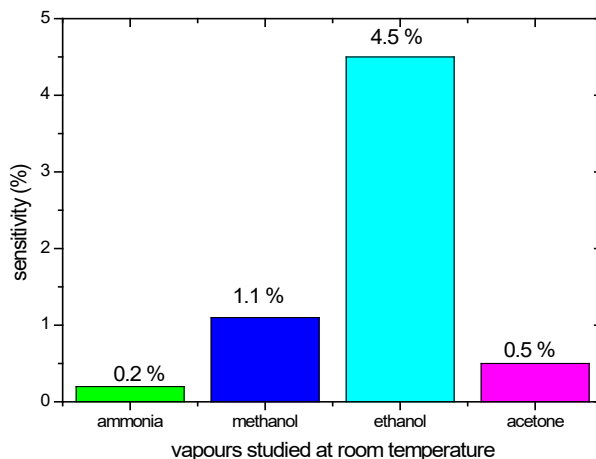


Fig. 7. Selectivity amidst various volatile vapours by $\text{MoO}_3 - \text{MoO}_2$ composite.

3.4. Mechanism

$\text{MoO}_3 - \text{MoO}_2$, an n-type metal oxide semiconductor with lots of lattice oxygen vacancies. Since gas sensing depends on the surface adsorbed oxygen molecules so here surface oxygen vacancies (interstitial oxygen and oxygen vacancies) play the main role. There is a coexistence of interstitial oxygen and oxygen vacancies for a surface defective site in the composite [29, 30]. On the interaction of these oxygen defects with the ethanol, there is a release of free electrons in the conduction band. This oxygen vacancy activates the $-\text{CO}$ and OH bond of ethanol and dehydrogenation takes place [29, 31 - 32]. This will, in turn, increase the free electron concentration in the conduction band and hence the resistance decreases. The observed small response of the composite material $\text{MoO}_3 - \text{MoO}_2$ towards ethanol might be due to the large sized fibrils and further reduction in size along with homogenous phase has to be yet achieved to have better sensing ability with shorter response – recovery characteristics.

4. Conclusion

$\text{MoO}_3 - \text{MoO}_2$ composite prepared via hydrothermal method is confirmed by the phase composition observed from XRD and the FESEM image reveals the aggregation of nanofibrils resulted in microrods. The sample exhibits ethanol sensing ability and the sensitivity is obtained as 4.5 % towards 25 ppm of ethanol and is highly selective to ethanol when compared to other vapours. The longer response time and recovery time could be attributed to the larger sized grains of the composite material.

References

- [1] Lu Wang, Meng-Chao Li, Guo -Hua Zhang, Zheng -Liang Xue, High Temperature Materials and Processes 39, 620 -626 (2020); <https://doi.org/10.1515/htmp-2020-0093>
- [2] Jie Dang, Guo-Hua Zhang, Kuo-Chih Chou, Ramana G. Reddy, Yu He, Yuanjun Sun, Int. Journal of Refractory Metals and Hard Materials 41, 216-223 (2013); <https://doi.org/10.1016/j.jirmhm.2013.04.002>
- [3] H. C. Xuan, Y. Q. Zhang, Y. K. Xu, H. Li, P. D. Han, D. H. Wang, Y. W. Du, Phys. Status Solidi A, 213 (9), 2468-2473 (2016); <https://doi.org/10.1002/pssa.201533069>
- [4] Daseul Han, Sooyeon Hwang, Seong-Min Bak, Kyung-Wan Nam, Electrochimica Acta 388 138635 (2021); <https://doi.org/10.1016/j.electacta.2021.138635>

- [5] Jiangfeng Ni, Guibin Wang, Juan Yang, Dongliang Gao, Jitao Chen, Lijun Gao, Yan Li, *Journal of Power Sources* 247, 90-94 (2014); <https://doi.org/10.1016/j.jpowsour.2013.08.068>
- [6] Mohammadreza Nematollahi, Sverre M. Selbach, Tor Grande, Fride Vullum-Bruer, *Thin Solid Films* 626, 94 -103 (2017); <https://doi.org/10.1016/j.tsf.2017.02.029>
- [7] Fengjuan Miao, Wenyi Wu, Qianqian Li, Rui Miao, Bairui Tao, *Int. J. Electrochem. Sci.*, 12 12060 - 12073 (2017); <https://doi.org/10.20964/2017.12.200>
- [8] Gennady Gorokh, Anna Zakhlebayev, Andrei Lazavenk, Nikolai Sobolev, Valery Zhyllinski, Nataliya Bogomazova, Marta Yarmolich, Nikolai Kalanda, *Physica status solidi b-basic solid state physics* (2019); <https://doi.org/10.1002/pssb.201900283>
- [9] Bin Hu, Liqiang Mai, Wen Chen, and Fan Yang, *ACS Nano*, 3 (2), 478-482 (2009); <https://doi.org/10.1021/nn800844h>
- [10] Yuping Chen, Chunliang Lu, Lin Xu, Ying Ma, Wenhua Hou, Jun-Jie Zhu, *CrystEngComm*, 12, 3740-3747 (2010); <https://doi.org/10.1039/c000744g>
- [11] Nallappan Maheswari, Gopalan Muralidharan, *Applied Surface Science* 416, 461-469 (2017); <https://doi.org/10.1016/j.apsusc.2017.04.094>
- [12] E. Comini, L. Yubao Y. Brando, G. Sberveglieri, *Chemical Physics Letters* 407, 368-371 (2005); <https://doi.org/10.1016/j.cplett.2005.03.116>
- [13] Sucheta Sau, Sonam Chakraborty, Tanushri Das and Mrinal Pal, *Frontiers in Materials* 6, 285 (2019); <https://doi.org/10.3389/fmats.2019.00285>
- [14] Lu Wang, Zheng-Liang Xue, Ao Huang, Fang-Fang Wang, *ACS Omega* 4, 20036–20047 (2019); <https://doi.org/10.1021/acsomega.9b03171>
- [15] A.S. Mohammed, S.O. Abdulghani, *Digest Journal of Nanomaterials and Biostructures* 17 (4), 1345-1352 (2022); <https://doi.org/10.15251/DJNB.2022.174.1345>
- [16] M. Chitra, K. Uthayarani, N. Rajasekaran, N. Neelakandeswari, E. K. Girija, D. Pathinettam Padiyan, G. Mangamma, *RSC Advances* 6, 111526 (2016); <https://doi.org/10.1039/C6RA24047J>
- [17] S. R. Cynthia, R. Sivakumar, C. Sanjeeviraja, C. Gopalakrishnan, K. Jeyadheepan, *J Mater Sci: Mater Electron* 31(20), 18018-18036 (2020); <https://doi.org/10.1007/s10854-020-04353-z>
- [18] Sameeh Mohamed Sali, Soumya Joy, N. Meenakshisundaram, Rakesh Kumar Karn, C. Gopalakrishnan, P. Karthick, K. Jeyadheepan, Kamatchi Sankaranarayanan, *RSC Adv.* 7, 37720 (2017); <https://doi.org/10.1039/C7RA05217K>
- [19] T. Nagyné-Kovács et al., *Nanomaterials* 10, 5, 2-13 (2020); <https://doi.org/10.3390/nano10050891>
- [20] Y. Liu, S. Yang, Y. Lu, N. V. Podval'naya, W. Chen, G. S. Zakharova, *Appl. Surf. Sci.* 359, 114-119 (2015); <https://doi.org/10.1016/j.apsusc.2015.10.071>
- [21] S. Sau, S. Chakraborty, T. Das, M. Pal, *Front. Mater.* 6, 1-6 (2019); <https://doi.org/10.3389/fmats.2019.00285>
- [22] N. Dukstiene, D. Sinkeviciute, A. Guobiene, *Cent. Eur. J. Chem.* 10 (4), 1106-1118 (2012); <https://doi.org/10.2478/s11532-012-0012-7>
- [23] Sapan Kumar Sen, Seema Dutta & Md. Razib Khan & M. S. Manir & Supria Dutta, Abdul Al Mortuza & Sultana Razia & M. A. Hakim, *BioNanoScience* (2019); <https://doi.org/10.1007/s12668-019-00671-7>
- [24] Nemat Tahmasebi, Marzieh Khalildashti, *Korean J. Chem. Eng.* 37(3), 448-455 (2020); <https://doi.org/10.1007/s11814-019-0469-6>
- [25] Noe Zamora-Romero, Miguel A. Camacho-Lopez, Alfredo R. Vilchis-Nestor, Victor H. Castrejon-Sanchez, Guillermo Aguilar, Santiago Camacho-Lopez, Marco Camacho-Lopez, *Materials Chemistry and Physics*, 240, 122163 (2020); <https://doi.org/10.1016/j.matchemphys.2019.122163>
- [26] Hanmei Hu, Junchan Xu, Chonghai Deng, Xinqing Ge, *Journal of Nanoscience and Nanotechnology* 14, 4462-4468 (2014); <https://doi.org/10.1166/jnn.2014.8287>

- [27] M. B. Sreedhara, H. S. S. Ramakrishna Matte, A. Govindaraj, C. N. R. Rao, *Chem. Asian J.* 8(10), 2430-2435 (2013); <https://doi.org/10.1002/asia.201300470>
- [28] Di Wu, Rui Shen, Rong Yang, Wenxu Ji, Meng Jiang, Weiping Ding, Luming Peng, *Scientific Reports* 7, 44697 (2017); <https://doi.org/10.1038/srep44697>
- [29] Uttam Kumar Sena, Sagar Mitra, *Energy Procedia* 54, 740 - 747 (2014); <https://doi.org/10.1016/j.egypro.2014.07.315>
- [30] Hao Xu, Liangjing Zhang, Aiwu Wang Juan Hou, Xuhong Guo, *Nanomaterials* 11, 3192 (2021); <https://doi.org/10.3390/nano11123192>
- [31] O. de Melo, Y. González, A. Climent-Font, P. Galán, A. Ruediger, M. Sánchez, C. Calvo, G. Santana, V. Torres-Costa, *J. Phys.: Condens. Matter* 31, 295703 (2019); <https://doi.org/10.1088/1361-648X/ab18e2>
- [32] David O. Scanlon, Graeme W. Watson, D. J. Payne, G. R. Atkinson, R. G. Egdell, D. S. L. Law, *J. Phys. Chem. C* 114, 4636-4645 (2010); <https://doi.org/10.1021/jp9093172>